# Synthesis of novel L-cysteine-modified TiO$_2$–In$_2$O$_3$ composites by the sol–gel method: evaluating surface characteristics and photocatalytic activity

Jui-Tai Wu[a], Chao-Yin Kuo[b], Chung-Hsin Wu[a],*

[a]*Department of Chemical and Materials Engineering, National Kaohsiung University of Applied Sciences, 415 Chien Kung Road, Kaohsiung, Taiwan, Tel. +886 7 3814526, ext 5137; email: wrt@kuas.edu.tw (J.-T. Wu), Tel. +886 7 3814526, ext 5158; Fax: +886 7 3830674; email: wuch@kuas.edu.tw (C.-H. Wu)*
[b]*Department of Environmental and Safety Engineering, National Yunlin University of Science and Technology, 123 University Road, Sec. 3, Douliou, Yunlin, Taiwan, Tel. +886 5 5342601, ext 4423; email: kuocyr@ms35.hinet.net*

## ABSTRACT

This study applied the sol–gel method to generate TiO$_2$–In$_2$O$_3$ composites (Ti–In), and this prepared Ti–In was further modified with L-cysteine to form S–N co-doped Ti–In (Ti–In–SN). Surface properties of the Ti–In–SN were analyzed by X-ray diffraction, UV–vis spectrophotometry, scanning electron microscopy, transmission electron microscopy, surface area analysis, and X-ray photoelectron spectroscopy. The dye C.I. reactive red 2 (RR2) was utilized as the model compound subjected to Ti–In and Ti–In–SN and measured for removal by adsorption and photocatalytic degradation. The Ti–In–SN had an average diameter of 13 nm, surface area of 48.6 m$^2$/g, and band gap energy of 2.75 eV. Removal rate constants for RR2 in the UV/Ti–In and UV/Ti–In–SN systems fitted pseudo-first-order kinetics and were 0.43 and 0.68 h$^{-1}$, respectively. Co-doping S–N in Ti–In via L-cysteine formed Ti–N–O, Ti–O–N, and Ti–O–S bonds; hence, crystalline size and band gap energy were decreased. Accordingly, adsorption ability and photocatalytic activity of Ti–In–SN for RR2 decolorization was improved.

*Keywords:* TiO$_2$; In$_2$O$_3$; L-cysteine; Co-doping; Photocatalysis

## 1. Introduction

Advanced oxidation processes effectively decolorize and eliminate the pollutants in textile wastewater. Titanium dioxide (TiO$_2$) is currently considered as the most promising photocatalyst because of its chemical and biological stability, high availability, and nontoxicity. However, when the amount of available oxygen in a solution is limited, rapid recombination of photogenerated electrons and holes in TiO$_2$ reduces the efficiency of photocatalytic reactions.

Notably, TiO$_2$ can be modified by combining it with metal oxides and doping it with nonmetals to reduce its band gap energy, extend the life and utility of photogenerated electron-hole pair, or improve pollutant adsorption on the catalyst surface. Many studies have combined TiO$_2$ with In$_2$O$_3$ to produce TiO$_2$–In$_2$O$_3$ composites (Ti–In) via the sol–gel approach [1–4]. These studies showed that organic removal efficiency of Ti–In exceeds that of TiO$_2$. This process effectively captures photogenerated electrons and

*Corresponding author.

retards the recombination of photogenerated electron-hole pairs [4,5]. Nonmetal-doped forms of $TiO_2$, such as N-doped $TiO_2$ [6–8] and S-doped $TiO_2$ [9–11], exhibit superior photocatalytic activity because the N and S atoms effectively narrows the band gap energy of $TiO_2$. Moreover, S–N co-doped $TiO_2$ [12–14] has been investigated and co-doped $TiO_2$ has been shown to have a higher photocatalytic activity than single-doped $TiO_2$ [6,13].

Several studies used thiourea as the dopant in modifying $TiO_2$ to generate S–N co-doped $TiO_2$ [13–16]. However, thiourea, a toxic chemical, is not an environmentally friendly reagent. Recently, biomolecule-assisted synthesis has been developed into novel methods for preparing various nanomaterials [17–19]. Hence, this study selected the L-cysteine (2-amino-3-sulfhydrylpropanoic acid), a biomolecule, as the dopant to modify the Ti–In surface. To the best of our knowledge, this is the first work to prepare S–N co-doped Ti–In (Ti–In–SN) using L-cysteine as the dopant. To assess the photocatalytic activities of Ti–In–SN, removal of C.I. reactive red 2 (RR2), a common azo dye, was studied. The objectives of this study were to (i) characterize the surface properties of Ti–In–SN, and (ii) assess the photocatalytic activity of Ti–In–SN in decolorizing RR2 relative to the parent Ti–In.

## 2. Materials and methods

### 2.1. Materials

The sources of Ti and In for preparing Ti–In were $TiCl_4$ (Acros) and $InCl_3$ (Alfa Aesar), respectively. The parent compound was RR2 ($C_{19}H_{10}Cl_2N_6Na_2O_7S_2$) and the dopant was L-cysteine ($C_3H_7NO_2S$), respectively, and both were obtained from Sigma-Aldrich. Single-doping S or N into Ti–In under the same mole ratio was performed to generate Ti–In–S or Ti–In–N. Their effectiveness was then compared with that of Ti–In–SN. The precursor of S and N was sodium thiosulfate and urea for Ti–In–S and Ti–In–N, respectively. Solution pH was adjusted using 0.1 M $HNO_3$ (Merck) and 0.1 M NaOH (Merck). All chemicals were of analytical reagent grade and used as obtained.

### 2.2. Preparation of photocatalysts

The Ti–In was prepared with a Ti/In mole ratio of 54 via the sol–gel method, as described previously [4]. Experimental results reported for Ti–In by Wu et al. [4] were used as background data to compare with the experimental results for Ti–In–SN obtained herein. L-cysteine (1.179 g) was first mixed with 20 mL HCl (0.65 M) by placing the mixture in an ultrasonic bath

for 10 min, then $InCl_3$ (0.4805 g; 99.9%) and $TiCl_4$ (13 mL; 98%) were added to this solution. Solution pH was adjusted by adding 26 mL $NH_4OH$ solution (28%), forming a yellow solid precipitate. Rengifo-Herrera et al. [15] demonstrated that photocatalytic activity of co-doped powders decreased when calcination temperature exceeded 500°C. Hence, the precipitate was collected by filtration and washed repeatedly with distilled water; it was dried at 110°C for 24 h and then calcined at 450°C for 2 h to yield the Ti–In–SN. The Ti/SN mole ratio was 11.9. To produce Ti–In–S, except for changing the precursor from L-cysteine to sodium thiosulfate (0.771 g), all procedures were same as that to generate Ti–In–SN. To prepare Ti–In–N, Ti–In (2.5 g) and urea (0.074 g) were thoroughly mixed and the mixture was then calcined at 450°C for 2 h.

### 2.3. Characterization

The crystalline structure of prepared photocatalysts was analyzed by X-ray diffraction (XRD) (Bruker D8 SSS, Germany). Accelerating voltage was 40 kV and applied current was 30 mA. The XRD patterns were recorded as $2\theta$ values in the range of 10–90°. The specific surface area of samples was determined using nitrogen as the adsorbate at −196°C in a static volumetric apparatus (Micromeritics ASAP 2020, USA). The UV–vis spectroscopy (JAS.CO-V670, Japan) was applied to profile absorbance spectra of photocatalysts at wavelengths of 200–800 nm. The UV–vis diffuse reflectance spectra were utilized to calculate the band gap energy of photocatalysts. The morphology and structure of Ti–In–SN were characterized using scanning electron microscopy (SEM) (JEOL 6330 TF, Japan) and transmission electron microscopy (TEM) (JEOL 3010, Japan). The X-ray photoelectron spectroscopy (XPS) measurements were taken using a PHI Quantum 5000 XPS system (USA) with a monochromatic Al Kα source and a charge neutralizer. The $C_{1s}$ peak at 284.5 eV was used to calibrate the spectra.

### 2.4. Decolorization of RR2

Experiments used 0.2 g/L of each photocatalyst at pH 3 and 25°C. In total, 20 mg/L RR2 was used in all experiments, except those to determine the concentration effect of RR2 on its decolorization. Decolorization experiments were carried out in a 3-L hollow cylindrical glass reactor, illuminated by an 8-W UV lamp (254 nm, Philips) with a light intensity of 1.12 W/m$^2$ that was placed inside a quartz tube. Adsorption experiments were performed in darkness. The reaction medium was stirred continuously at 300 rpm to keep it in suspension. Aliquots, with a total volume of

10 mL, were withdrawn from the reactor at preset time intervals to assess reaction progress. Following the sampling, solids were separated by filtration through a 0.22 μm filter (Millipore), and the RR2 remaining in the filtrate was analyzed by a spectrophotometer using absorbance at 538 nm (Hitachi U-5100, Japan).

## 3. Results and discussion

### 3.1. Surface characteristics of Ti–In and Ti–In–SN

Fig. 1 shows the XRD patterns of Ti–In and Ti–In–SN. The peaks, diffractions of various crystal planes of anatase, were at 25.4°, (1 0 1) and 48.1°, (2 0 0). Other crystal phases corresponding to peaks at 27.4°, 36.1°, 41.2°, and 54.3° were the diffraction peaks of (1 1 0), (1 0 1), (1 1 1), and (2 1 1) of rutile, respectively. No patterns included any $In_2O_3$, N-derived, or S-derived peaks. One reason for this absence was that the L-cysteine concentration was so low that it was undetectable by XRD. The other was that N and S atoms in L-cysteine were incorporated into the structure of Ti–In and substituted the lattice oxygen and titanium atoms or located at the interstitial sites. Anatase content was determined from the intensity of (1 0 1) anatase diffraction, $I_A$, and that of (1 1 0) rutile diffraction, $I_R$, using Eq. (1) [20]. With these XRD patterns, the crystalline size of prepared powders was calculated using Scherrer's formula, Eq. (2):

$$\text{Anatase} \quad (\%) = \frac{1}{1 + 12.6\frac{I_A}{I_R}} \times 100 \qquad (1)$$
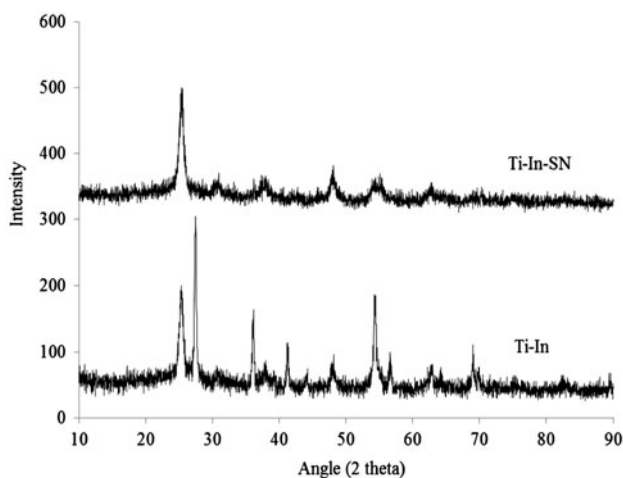


Fig. 1. XRD pattern of Ti–In and Ti–In–SN.

$$D = \frac{0.9\lambda}{\beta \cos \theta} \qquad (2)$$

where $D$ is the crystalline size in nm, $\lambda$ is the X-ray wavelength (0.15418 nm), $\beta$ is the line width at medium height of the anatase (1 0 1) and rutile (1 1 0) peaks, and $\theta$ is the diffraction angle [21]. Table 1 lists the surface characteristics of Ti–In and Ti–In–SN. The anatase percentage of Ti–In–SN exceeded that of Ti–In. The XRD diagrams indicate that S–N co-doping retards transformation of the $TiO_2$ phase from anatase to rutile. Wang et al. [17] suggested adding L-cysteine favored the formation of anatase and inhibited the formation of rutile. This retardation may be due to stabilization of the anatase phase by the surrounding N and/or S ions. Hurum et al. [22] proposed that anatase has more stable electron-trapping sites than rutile, such that anatase exhibits more photocatalytic activity. Accordingly, S–N co-doping in Ti–In may improve the photocatalytic activity of Ti–In.

Particle size and band gap energy of Ti–In was greater than that of Ti–In–SN; conversely, the surface area of Ti–In was smaller than that of Ti–In–SN (Table 1). S–N co-doping in Ti–In reduced particle diameter, suggesting that S–N co-doping retards the agglomeration of Ti–In crystals; accordingly, the surface area of Ti–In–SN was further enlarged. Liu et al. [11] indicated that S-doping effectively inhibited the growth of $TiO_2$ crystals; Chen et al. [6] reported that N-doping had a similar effect. Wang et al. [17] also demonstrated that the addition of L-cysteine could decrease average crystalline size of the samples.

The band gap energy of Ti–In declined after S–N co-doping (Table 1). A red shift indicates that the Ti–In–SN can be excited to generate additional hole-electron pairs under UV-irradiation, which can increase photocatalytic activity. Li et al. [13] found that absorption spectra of S–N co-doped $TiO_2$ had a red shift in the adsorption edge. This shift was attributed to the fact that calcination induces doping

Table 1
Surface characteristics of prepared photocatalysts

| Photocatalysts | Ti–In[a] | Ti–In–SN |
|---|---|---|
| Anatase (%) | 30 | 100 |
| Rutile (%) | 70 | 0 |
| Particle size (nm) | 57 | 13 |
| BET (m²/g) | 35.7 | 48.6 |
| Band gap (eV) | 2.97 | 2.75 |

[a]Wu et al. [4].

of S and N atoms into the lattice of $TiO_2$, narrowing the band gap. The band gap energy for Ti–In–SN herein was similar to that for S–N co-doped $TiO_2$. Fig. 2(a) and (b) show SEM and TEM micrographs for Ti–In–SN, respectively. The Ti–In–SN exhibited a high tendency to agglomerate and had a platelet-like structure (Fig. 2(a)); moreover, the compact aggregates of Ti–In–SN sized 15–80 nm (Fig. 2(b)).

Fig. 3(a)–(e) present the XPS spectra of $Ti_{2p}$, $In_{3d}$, $O_{1s}$, $N_{1s}$, and $S_{2p}$, respectively, for Ti–In–S–N. The $Ti_{2p3/2}$ and $Ti_{2p1/2}$ spin-orbital-splitting photoelectrons were located at binding energies of 455.7–458.8 and 462.1–464.5 eV [23–25], respectively (Fig. 3(a)). These binding energies are close to those reported for $Ti^{4+}$ show binding energy in $TiO_2$ [26]. Both $In_{3d5/2}$ and $In_{3d3/2}$ spin-orbital splitting photoelectrons were observed at binding energies of 443.9–445 [24,27–29] and 451.5–452.0 eV [24,27,29], respectively (Fig. 3(b)). Peaks at 529.3, 529.7, and 531.1 eV were assigned to $O_{1s}$, and they were associated with In–O, Ti–O, and $OH^-$, respectively [28] (Fig. 3(c)).

Binding energies of 397.0–397.4 in the $N_{1s}$ region were assigned to Ti–N–O [30–32]; the binding energy at 399–400.7 eV was attributed to the Ti–O–N bond [24,28]. Moreover, binding energy of 402 eV in the $N_{1s}$ region was assigned to NO species [15,28] (Fig. 3(d)). Li et al. [13] indicated that the $N_{1s}$ peak at 402 eV was due to adsorbed organic impurities. The S atoms in this study were in the $S^{6+}$ state, yielding a peak at 168.2–169 eV [9,11,33] (Fig. 3(e)). When S atoms replace O atoms on $TiO_2$ surfaces, no peak exists in the range of 160–163 eV, which corresponds to the Ti–S bond [9]. Umebayashi et al. [34] suggested that sulfur was doped as an anion and replaced the lattice oxygen in $TiO_2$ to form Ti–S bonds; conversely, Ohno et al. [33] reported that S atoms were incorporated as cations and replaced Ti ions in the S-doped $TiO_2$. Anionic S-doping may be difficult to perform because $S^{2-}$ (0.17 nm) has a significantly larger ionic radius than $O^{2-}$ (0.122 nm). Hence, the substitution of $Ti^{4+}$ by $S^{6+}$ is chemically more favorable for Ti–In–SN than replacing $O^{2-}$ with $S^{2-}$ [9]. Cheng et al. [16] found that S elements were incorporated into the lattice of $TiO_2$ through substituting titanium atom and co-existed in the cationic forms $S^{6+}$ and $S^{4+}$. Ho et al. [10] suggested that the oxidation state of the S-dopant depends on the preparation route. Thus, XPS characterization confirmed that Ti–N–O, Ti–O–N, and Ti–O–S formed in Ti–In–SN in this study.

### 3.2. Photocatalytic activity of Ti–In–SN

At pH 3, no significant RR2 decolorization occurred during direct photolysis (<5%) (data not shown). Hence, the elimination of RR2 was attributed to adsorption and/or photodegradation reactions. Fig. 4 plots RR2 removal rates in the Ti–In, Ti–In–S, Ti–In–N, and Ti–In–SN systems. After 180 min, the Ti–In, Ti–In–S, Ti–In–N, and Ti–In–SN systems adsorbed 34, 24, 31, and 52% of RR2, and total removal percentages were 78, 55, 66, and 90%, respectively. The adsorption process was rapid in the initial 60 min, and then gradually decreased in speed until equilibrium was reached (Fig. 4). The pseudo-second-order model [35,36] was applied to analyze experimental data and thereby elucidate adsorption process kinetics. Equation (3) is the pseudo-second-order model, where $q_e$ and $q$ are the amounts of RR2 adsorbed onto the photocatalyst at equilibrium and at various times $t$ (mg/g), and $k_2$ is the rate constant of the pseudo-second-order model for adsorption (g/mg min).

$$\frac{t}{q} = \frac{1}{k_2 q_e^2} + \frac{t}{q_e} \tag{3}$$

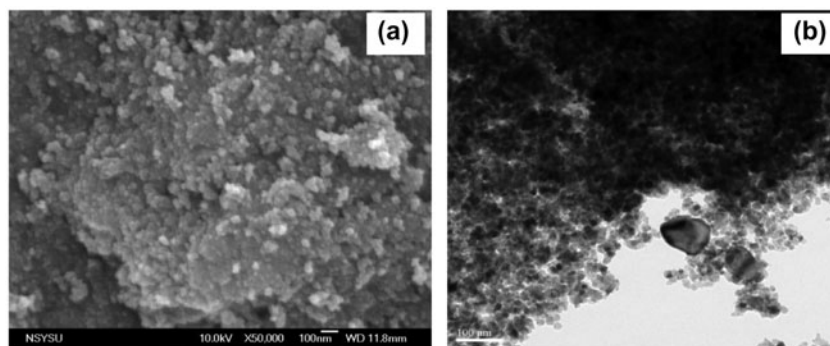Table 2 lists the kinetics parameters of various photocatalysts. The $R^2$ value of the pseudo-second-order
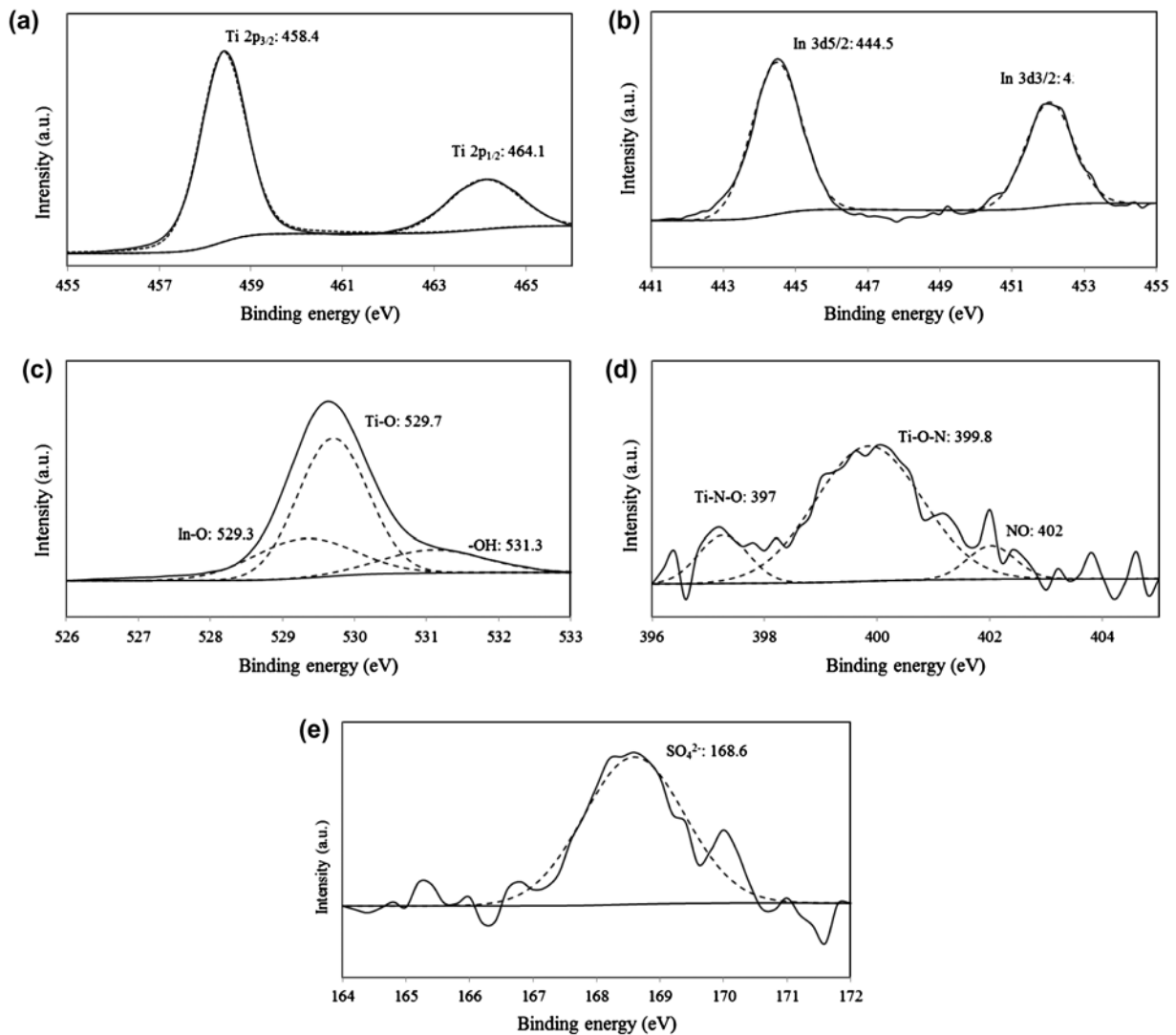


Fig. 2. Micrographs of Ti–In–SN (a) SEM and (b) TEM.

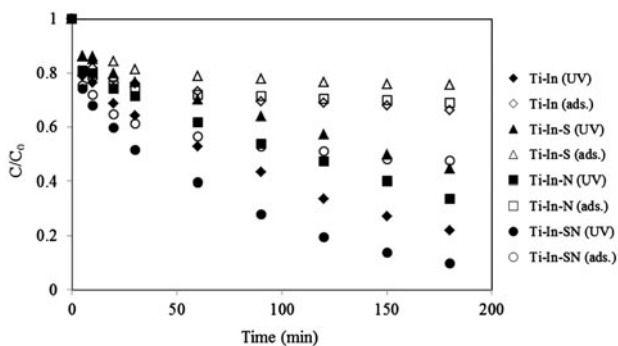Fig. 3. XPS spectra of Ti–In–SN (a) $Ti_{2p}$, (b) $In_{3d}$, (c) $O_{1s}$, (d) $N_{1s}$, and (e) $S_{2p}$.



Fig. 4. RR2 removal in Ti–In, Ti–In–S, Ti–In–N, and Ti–In–SN systems ([photocatalyst] = 0.2 g/L, [RR2] = 20 mg/L, pH 3).

model exceeded 0.995; moreover, the $q$ value ($q_{e,cal}$) derived from this pseudo-second-order model agreed well with experimental $q$ values ($q_{e,exp}$) (Table 2). Hence, the pseudo-second-order model well represents adsorption kinetics. The RR2 adsorption capacity of various photocatalysts followed the order Ti–In–SN > Ti–In > Ti–In–N > Ti–In–S. Moreover, the total removal rate constants ($k$) of RR2 in the tested systems fit pseudo-first-order kinetics, as in various dye decolorization studies [4,7]. The $k$ values followed the order Ti–In–SN > Ti–In > Ti–In–N > Ti–In–S (Table 2). The $k$ value trend agreed with the order of adsorption capacity of photocatalyst. Lv et al. [19] suggested that enhanced adsorption of the dye by L-cysteine-modified $TiO_2$ should also benefit dye photodegradation. Since the adsorption capacity of RR2 by Ti–In–S and Ti–In–N

Table 2
Kinetics parameters of various photocatalysts

| Photocatalysts | $k_2$ (g/mg min) | $q_{e, exp.}$ (mg/g) | $q_{e, cal.}$ (mg/g) | $k$ (h$^{-1}$) |
|---|---|---|---|---|
| Ti–In | $2.1 \times 10^{-3}$ (0.997) | 33.7 | 35.3 | 0.43 (0.999) |
| Ti–In–S | $4.1 \times 10^{-3}$ (0.998) | 24.3 | 25.4 | 0.22 (0.996) |
| Ti–In–N | $5.4 \times 10^{-3}$ (0.999) | 31.0 | 31.3 | 0.29 (0.998) |
| Ti–In–SN | $1.6 \times 10^{-3}$ (0.997) | 52.4 | 54.9 | 0.68 (0.999) |

Note: (): $R^2$ value.

was lower than that of Ti–In, single-doping S or N into Ti–In did not enhance the photocatalytic activity of Ti–In at the molar ratio of 11.9. The crystalline size of Ti–In was greater than Ti–In–SN; however, the k value of Ti–In–SN was higher than Ti–In. In large photocatalyst particles, the recombination process is reportedly favored since electrons and holes cannot easily reach the surface of photocatalyst within their lifetimes, limiting the formation of surface reactive oxidative species [15].

Both N and S atoms were incorporated into the lattice of Ti–In simultaneously, and were substituted for the lattice oxygen and titanium atoms, respectively, thereby inducing the formation of a new energy level and narrowing of the band gap. Cheng et al. [16] indicated that decoration with N–S co-doped $TiO_2$ markedly enhanced electron transfer and mobility by reducing the recombination of photogenerated electron and hole pairs; hence, degradation efficiency for organic pollutants was improved. Experimental results suggest that enhanced photocatalytic activity of L-cysteine-modified Ti–In was attributed to the synergistic effects of enhanced adsorption of organic pollutants and increased efficiency in separation of photogenerated electron and hole pairs, similar to the L-cysteine-modified $TiO_2$ [19].

Fig. 5 presents the RR2 removal in the UV/Ti–In–SN system under various RR2 concentrations. After 180 min, removal of RR2 from initial concentrations of 10, 20, and 40 mg/L by UV/Ti–In–SN was 96, 90, and 37%, respectively. The k value of 10, 20, and 40 mg/L RR2 was 1.66, 0.68, and 0.11 h$^{-1}$, respectively. The RR2 removal rate constants were inversely related to RR2 concentration. Increasing the RR2 concentration would to some extent shield the photocatalytically active sites from a given photon flux, reduce RR2 conversion. Additionally, increasing the amount of RR2, correspondingly intermediates may have increased the competition for photogenerated hydroxyl radicals. Thus, with the same amount of photocatalysts and photon input and an increased RR2 load, RR2 removal could be reduced due to shielding or increased consumption of hydroxyl radicals.
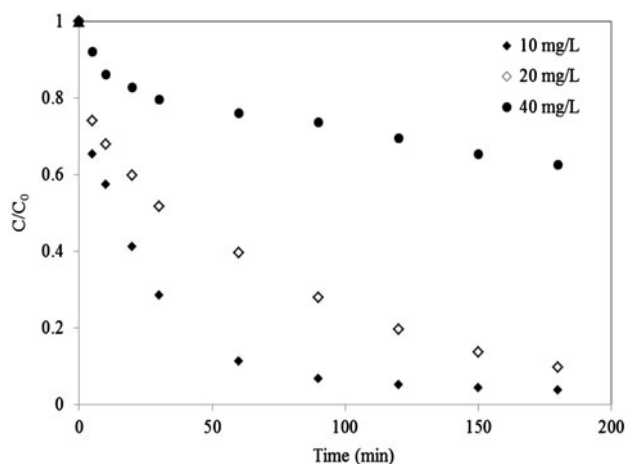


Fig. 5. Effects of RR2 concentration in UV/Ti–In–SN system ([Ti–In–SN] = 0.2 g/L, [RR2] = 20 mg/L, pH 3).

## 4. Conclusions

This study synthesized novel L-cysteine-modified $TiO_2$–$In_2O_3$ composites by the sol–gel method. Adding L-cysteine facilitated the formation of anatase and inhibited the formation of rutile. Moreover, S–N co-doping retarded the agglomeration of Ti–In crystals; hence, the surface area of Ti–In–SN was further enlarged. Both N and S atoms were incorporated into the lattice of Ti–In simultaneously, inducing the formation of a new energy level and narrowing the band gap. Experimental results suggest that the enhanced photocatalytic activity of Ti–In–SN was due to the synergistic effects of enhanced adsorption of RR2 and increased efficiency in separation of photogenerated electrons and holes. The RR2 decolorization rate decreased as the RR2 concentration increased.

Mr Lai and Chung of National Kaohsiung University of Applied Sciences are appreciated for assistance in conducting some of experiments.

## References

[1] D. Shchukin, S. Poznyak, A. Kulak, P. Pichat, TiO$_2$-In$_2$O$_3$ photocatalysts: Preparation, characterisations and activity for 2-chlorophenol degradation in water, J. Photochem. Photobiol., A 162 (2004) 423–430.

[2] V. Rodríguez-González, A. Moreno-Rodríguez, M. May, F. Tzompantzi, R. Gómez, Slurry photodegradation of 2,4-dichlorophenoxyacetic acid: A comparative study of impregnated and sol–gel In$_2$O$_3$–TiO$_2$ mixed oxide catalysts, J. Photochem. Photobiol., A 193 (2008) 266–270.

[3] L.C. Chen, C.M. Huang, C.S. Gao, G.W. Wang, M.C. Hsiao, A comparative study of the effects of In$_2$O$_3$ and SnO$_2$ modification on the photocatalytic activity and characteristics of TiO$_2$, Chem. Eng. J. 175 (2011) 49–55.

[4] C.H. Wu, C.Y. Kuo, C.H. Lai, W.Y. Chung, Surface characteristics and photocatalytic properties of TiO$_2$–In$_2$O$_3$ composite powders by using the sol–gel method: Effects of preparation conditions, React. Kinet. Mech. Catal. 112 (2014) 543–557.

[5] F. Ma, S. Zhang, X. Yang, W. Guo, Y. Guo, M. Huo, Fabrication of metallic platinum and indium oxide codoped titania nanotubes for the simulated sunlight photocatalytic degradation of diethyl phthalate, Catal. Commun. 24 (2012) 75–79.

[6] D. Chen, Z. Jiang, J. Geng, Q. Wang, D. Yang, Carbon and nitrogen co-doped TiO$_2$ with enhanced visible-light photocatalytic activity, Ind. Eng. Chem. Res. 46 (2007) 2741–2746.

[7] C.H. Wu, C.Y. Kuo, S.T. Chen, Synergistic effects between TiO$_2$ and carbon nanotubes (CNTs) in a TiO$_2$/CNTs system under visible light irradiation, Environ. Technol. 34 (2013) 2513–2519.

[8] C.Y. Kuo, Y.H. Yang, Exploring the photodegradation of bisphenol A in a sunlight/immobilized N-TiO$_2$ system, Pol. J. Environ. Stud. 23 (2014) 379–384.

[9] J.C. Yu, W. Ho, J. Yu, H. Yip, P.K. Wong, J. Zhao, Efficient visible-light-induced photocatalytic disinfection on sulfur-doped nanocrystalline titania, Environ. Sci. Technol. 39 (2005) 1175–1179.

[10] W. Ho, J.C. Yu, S. Lee, Low-temperature hydrothermal synthesis of S-doped TiO$_2$ with visible light photocatalytic activity, J. Solid State Chem. 179 (2006) 1171–1176.

[11] S.Y. Liu, Q.L. Tang, Q.G. Feng, Synthesis of S/Cr doped mesoporous TiO$_2$ with high active visible light degradation property via solid state reaction route, Appl. Surf. Sci. 257 (2011) 5544–5551.

[12] J. Yu, M. Zhou, B. Cheng, X. Zhao, Preparation, characterization and photocatalytic activity of in situ N, S-codoped TiO$_2$ powders, J. Mol. Catal. A: Chem. 246 (2006) 176–184.

[13] X. Li, R. Xiong, G. Wei, S–N co-doped TiO$_2$ photocatalysts with visible-light activity prepared by sol–gel method, Catal. Lett. 125 (2008) 104–109.

[14] J.A. Rengifo-Herrera, C. Pulgarin, Photocatalytic activity of N, S co-doped and N-doped commercial anatase TiO$_2$ powders towards phenol oxidation and E. coli inactivation under simulated solar light irradiation, Sol. Energy 84 (2010) 37–43.

[15] J.A. Rengifo-Herrera, E. Mielczarski, J. Mielczarski, N.C. Castillo, J. Kiwi, C. Pulgarin, Escherichia coli inactivation by N, S co-doped commercial TiO$_2$ powders under UV and visible light, Appl. Catal., B 84 (2008) 448–456.

[16] X. Cheng, H. Liu, Q. Chen, J. Li, P. Wang, Construction of N, S codoped TiO$_2$ NCs decorated TiO$_2$ nanotube array photoelectrode and its enhanced visible light photocatalytic mechanism, Electrochim. Acta 103 (2013) 134–142.

[17] Y. Wang, Y. Huang, W. Ho, L. Zhang, Z. Zou, S. Lee, Biomolecule-controlled hydrothermal synthesis of C-N-S-tridoped TiO$_2$ nanocrystalline photocatalysts for NO removal under simulated solar light irradiation, J. Hazard. Mater. 169 (2009) 77–87.

[18] L. Dong, S. Guo, S. Zhu, D. Xu, L. Zhang, M. Huo, X. Yang, Sunlight responsive BiVO$_4$ photocatalyst: Effects of pH on L-cysteine-assisted hydrothermal treatment and enhanced degradation of ofloxacin, Catal. Commun. 16 (2011) 250–254.

[19] K. Lv, J. Hu, X. Li, M. Li, Cysteine modified anatase TiO$_2$ hollow microspheres with enhanced visible-light-driven photocatalytic activity, J. Mol. Catal. A: Chem. 356 (2012) 78–84.

[20] R.A. Spurr, H. Myers, Quantitative analysis of anatase-rutile mixtures with an X-ray diffractometer, Anal. Chem. 29 (1957) 760–762.

[21] I.C. Kang, Q. Zhang, S. Yin, T. Sato, F. Saito, Preparation of a visible sensitive carbon doped TiO$_2$ photocatalyst by grinding TiO$_2$ with ethanol and heating treatment, Appl. Catal., B 80 (2008) 81–87.

[22] D.C. Hurum, A.G. Agrios, K.A. Gray, T. Rajh, M.C. Thurnauer, Explaining the enhanced photocatalytic activity of degussa P25 Mixed-Phase TiO$_2$ using EPR, J. Phys. Chem. B 107 (2003) 4545–4549.

[23] Q. Xiao, L. Ouyang, Photocatalytic activity and hydroxyl radical formation of carbon-doped TiO$_2$ nanocrystalline: Effect of calcination temperature, Chem. Eng. J. 148 (2009) 248–253.

[24] R. Sasikala, A.R. Shirole, V. Sudarsan, Enhanced photocatalytic activity of indium and nitrogen co-doped TiO$_2$–Pd nanocomposites for hydrogen generation, Appl. Catal., A 377 (2010) 47–54.

[25] X. Wang, T.T. Lim, Effect of hexamethylenetetramine on the visible-light photocatalytic activity of C-N codoped TiO$_2$ for bisphenol A degradation: Evaluation of photocatalytic mechanism and solution toxicity, Appl. Catal., A 399 (2011) 233–241.

[26] X. Wang, Z. Hu, Y. Chen, G. Zhao, Y. Liu, Z. Wen, A novel approach towards high performance composite photocatalyst of TiO$_2$ deposited on activated carbon, Appl. Surf. Sci. 255 (2009) 3953–3958.

[27] M. Tominaga, UV-ozone dry-cleaning process for indium oxide electrodes for protein electrochemistry, Electrochem. Commun. 7 (2005) 1423–1428.

[28] K.R. Reyes-Gil, E.A. Reyes-Garcia, D. Raftery, Nitrogen-doped In$_2$O$_3$ thin film electrodes for photocatalytic water splitting, J. Phys. Chem. C 111 (2007) 14579–14588.

[29] X. Yang, Y. Wang, L. Xu, X. Yu, Y. Guo, Silver and indium oxide codoped TiO$_2$ nanocomposites with

enhanced photocatalytic activity, J. Phys. Chem. C 112 (2008) 11481–11489.

[30] N.C. Saha, H.G. Tompkins, Titanium nitride oxidation chemistry: An X-ray photoelectron spectroscopy study, J. Appl. Phys. 72 (1992) 3072–3079.

[31] E. György, A.P. Pérez del Pino, P. Serra, J.L. Morenza, Depth profiling characterisation of the surface layer obtained by pulsed Nd:YAG laser irradiation of titanium in nitrogen, Surf. Coat. Technol. 173 (2003) 265–270.

[32] I.M. Ismail, B. Abdallah, M. Abou-Kharroub, O. Mrad, XPS and RBS investigation of $TiN_xO_y$ films prepared by vacuum arc discharge, Nucl. Instrum. Methods Phys. Res., Sect. B 271 (2012) 102–106.

[33] T. Ohno, M. Akiyoshi, T. Umebayashi, K. Asai, T. Mitsui, M. Matsumura, Preparation of S-doped $TiO_2$ photocatalysts and their photocatalytic activities under visible light, Appl. Catal., A 265 (2004) 115–121.

[34] T. Umebayashi, T. Yamaki, S. Yamamoto, A. Miyashita, S. Tanaka, T. Sumita, K. Asai, Sulfur-doping of rutile-titanium dioxide by ion implantation: Photocurrent spectroscopy and first-principles band calculation studies, J. Appl. Phys. 93 (2003) 5156–5160.

[35] G. Blanchard, M. Maunaye, G. Martin, Removal of heavy metals from waters by means of natural zeolites, Water Res. 18 (1984) 1501–1507.

[36] Y.S. Ho, G. McKay, Sorption of dye from aqueous solution by pit, Chem. Eng. J. 70 (1988) 115–124.